# Electrodeposition of Composition-Modulated Alloys in a Fluctuating Flow Field

The effect of fluctuating flow on the electrodeposition of binary alloys is analyzed by numerically solving the transient Navier-Stokes and species continuity equations for a rotating disk electrode system. Time-periodic modulations of the flow field and the electrode potential are studied and shown to induce periodic deposition rates for a mass-transfer-limited species and an activation-limited species, respectively. Dimensionless groups are formulated to characterize the operating regimes, where composition-modulated alloys electrodeposit from a single electrolyte and where fluctuating flow influences the composition distribution of the deposit. It is shown that changing the phase angle difference between the flow and potential modulation waveforms can modify the composition gradients in the deposited alloy, whereas other features of the alloy, such as the total composition variation, are affected less by fluctuating flow.

**D. T. Schwartz**
**P. Stroeve**
**B. G. Higgins**
Department of Chemical Engineering
University of California
Davis, CA 95616

## Introduction

Metallic alloys with spatially-periodic variations in composition often exhibit unusual mechanical (Tsakalakos and Jankowski, 1986), magnetic (Thaler et al., 1978; Bennett et al., 1987), electrical, and chemical properties (Cohen et al., 1983, 1984), especially when the periodicity in the composition variation is on the order of nanometers. Spatially periodic metallic thin films are referred to as composition-modulated alloys (CMA's) when the junction (also called the interphase) region between alternating layers is diffuse, i.e., the junction region is not discrete at the atomic level. Within the junction region, the composition of the alloy can have large gradients. Figure 1a is a schematic representation of a one-dimensional CMA with periodicity wavelength $L$.

Nanometer wavelength CMA's were initially fabricated in the late 1960's to test theories on the thermodynamic stability and interdiffusion of layered materials (Hilliard, 1970). Although vacuum evaporation techniques have been used to form reproducible, thin-film alloys with nearly sinusoidal composition variations (Jankowski and Tsakalakos, 1985), sputtering and electrodeposition techniques seem to be preferred methods for fabricating nanometer wavelength CMA's with narrow interphase regions (Negai et al., 1988; Tench and White, 1984).

Correspondence concerning this paper should be addressed to B. G. Higgins.
Current address of D. T. Schwartz: Materials and Chemical Sciences Division, Lawrence Berkeley Laboratory, 62-203, University of California, Berkeley, CA 94720.

Recent developments in the electrochemical fabrication of composition-modulated alloys have been oriented toward depositing materials with large composition gradients from a single electrolyte bath (Lashmore and Dariel, 1988). Experiments have shown that pulse-plated binary alloys often have periodic composition variations when the deposition of the more noble species (the species that deposits at a more positive potential) is mass-transfer-limited, and the deposition of the less noble species is activation-limited (Yahalom and Zadok, 1987). Periodic modulation of the electrode potential modulates the deposition rate of the activation-limited species, but not the mass-transfer-limited species. Conversely, periodic modulation of the electrolyte flow field modulates the deposition rate of the mass-transfer-limited species, but not the activation-limited species. A CMA forms when the deposition rate of one or both alloy species is time-periodic.

Several different pulse plating schemes and convective flow environments have been used by researchers to electrochemically fabricate CMA's. Brownlow (1966) electrodeposited modulated CuNiFe thin films consisting of 10 Å of nonmagnetic Cu-rich alloy and 110 Å of magnetic Cu-depleted alloy by pulsing the deposition current. During periods of zero applied current, the electrolyte was agitated mechanically. The structure of the alloy was deduced from the magnetic properties of the material. Tench and White (1984) and Menzes and Anderson (1988) electrochemically-deposited nanometer-scale modulated Cu-Ni alloys using potential (current) pulsing along with simultaneous

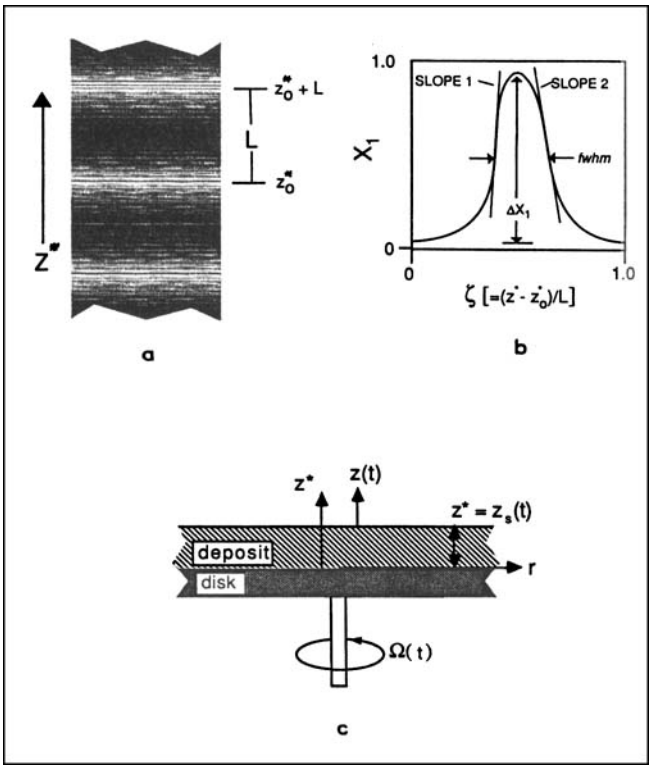


**Figure 1. Composition-modulated alloy with periodicity wavelength *L*.**

(a) One-dimensional CMA has composition modulations in the $z^*$ direction only, as shown by the gray scaling.

(b) Alloy unit cell mole fraction $X_1$ profile for the CMA in Figure 1a. The alloy full width at half maximum is denoted by *fwhm*. The largest positive and negative composition gradients are given by SLOPE 1 and SLOPE 2. $\Delta X_1$ is the total mole fraction variation over one unit cell.

(c) Fixed coordinate system is denoted by $z^*$ and moving coordinate system is denoted by $z$.

time-periodic fluctuating flow. With an etching technique, they showed that large composition gradients were present in the Cu-Ni electrodeposits. Yahalom and Zadok (1987) electrodeposited Cu-Ni CMA with periodicity wavelengths as low as 0.8 nm by pulsing the potential of a rotating disk electrode (RDE). The effect of changing the convective mass transfer rate was studied, and they found that the copper concentration in the deposit was proportional to the square root of the RDE angular velocity—a result consistent with copper (the more noble metal) deposition being mass-transfer-limited. Yahalom and Zadok used Auger spectroscopy and sputter etching to obtain composition profiles of their alloy thin films, but the resolution of the technique was insufficient to make quantitative measurements of the interphase gradients. Recently Lashmore and Dariel (1988) analyzed the crystallographic orientation of pulse-plated Cu-Ni modulated alloys deposited epitaxially on carefully prepared substrates and found lattice coherency.

The modeling of electrochemical CMA formation has not kept pace with experimental studies. Verbrugge and Tobias (1985, 1987) have modeled the pulse plating of alloy materials onto a RDE with constant angular velocity. Although the kinetic parameters and current pulsing scheme they considered did induce small amplitude composition modulations in the modeled deposits, the authors did not provide a detailed analysis of the operating conditions that produced pulse-plated CMA's. Ruffoni and Landolt (1988) used a model similar to Verbrugge and Tobias' to predict the composition of a ternary alloy pulse plated in a steady flow field. Those authors showed results that indicate that composition modulations were present in their modeled alloys, but the emphasis of their work was on the spatially-averaged alloy composition. Other models of alloy pulse plating have addressed issues such as migration effects (Pesko and Cheh, 1988), but none, to the best of our knowledge, have analyzed CMA electrodeposition or the effects of fluctuating flow on the composition gradients of the alloy.

In this paper we report the effects of fluctuating flow on the periodic electrodeposition of composition-modulated alloys. The deposition of Cu and Ni onto a rotating disk electrode with time-periodic, angular-velocity modulations is used as the model system. Kinetics rate parameters for the $Cu^{+2}$ and $Ni^{+2}$ reduction reactions are determined from experimental results available in the electrochemical literature. The time-dependent Navier-Stokes and species continuity equations are solved numerically to determine the deposition rate of each component of the alloy. We consider separately the effects of time-periodic flow, time-periodic potential modulations, and simultaneous potential and flow modulations on the formation of electrochemical CMA's. The Discussion section focuses on flow-induced modifications to the composition gradients in the interphase region of the alloy. It is shown that changing the phase angle difference between the potential and the flow modulations can modify the maximum composition gradients in the alloy by a factor of five at sufficiently low modulation frequencies. As the frequency increases, mass transfer relaxation effects are found to attenuate the influence of fluctuating flow on the resulting CMA deposit.

## Theory

### *Flow field*

In order to analyze the effects of time-periodic flow and potential on alloy electrodeposition, we consider the time-dependent mass transfer environment in the neighborhood of a rotating disk electrode. The RDE geometry is shown schematically in Figure 1c. Because of electrodeposition, the solid/electrolyte boundary undergoes an unsteady axial translation. Two coordinate frames are defined in Figure 1c: the inertial frame is fixed at the original ($t = 0$) interface, whereas the second frame of reference translates axially with the growing deposit. Quantities determined in the inertial frame are denoted by a superscript *. The two frames are related through the relationship

$$z^* = z + z_s^*(t), \quad r = r^*, \quad t = t^*, \tag{1}$$

where $z_s^*(t)$ is the thickness of the electrodeposit at any instant in time $t$. The flow field in the inertial frame is taken to be axisymmetric and self-similar (von Kármán, 1921):

$$v^* = rf^*(t, z^*)e_r + rg^*(t, z^*)e_\theta + h^*(t, z^*)e_z. \tag{2}$$

Substitution of Eq. 2 into the continuity and Navier-Stokes equations provides a set of coupled nonlinear partial-differential equations for $f^*$, $g^*$, and $h^*$ that are independent of radial position. The governing equations for $f^*$, $g^*$, and $h^*$ can be placed in the translating frame of reference by applying Eq. 1 and the

chain rule. In dimensionless form, these equations are

$$\frac{\partial H}{\partial \eta} + 2F = 0, \tag{3a}$$

$$\frac{\partial F}{\partial \tau} + F^2 - G^2 + H\frac{\partial F}{\partial \eta} = \frac{\partial^2 F}{\partial \eta^2}, \tag{3b}$$

$$\frac{\partial G}{\partial \tau} + 2FG + H\frac{\partial G}{\partial \eta} = \frac{\partial^2 G}{\partial \eta^2}, \tag{3c}$$

where $\tau = t\Omega_o$ is dimensionless time, and $\eta = z/\sqrt{\nu/\Omega_o}$ is the dimensionless axial distance measured from the solid/electrolyte interface. The components of velocity are made dimensionless with the mean angular velocity $\Omega_o$ of the RDE so that $G = g/\Omega_o$, $F = f/\Omega_o$, and $H = h/\sqrt{\nu/\Omega_o}$, where $\nu$ is the electrolyte kinematic viscosity. The hydrodynamic pressure can be calculated from the axial component of the momentum equation, but it is not needed for this study. In the translating frame, there is no slip or penetration of fluid at the solid/electrolyte interface. Thus

$$H(\tau, 0) = F(\tau, 0) = 0, \tag{4}$$

$$G(\tau, 0) = 1 + \alpha \cos(p\tau - \phi). \tag{5}$$

The fluctuating component of the flow is introduced through boundary condition (Eq. 5). The variable $\alpha$ is the rotation modulation amplitude; $p = \sigma/\Omega_o$ is the dimensionless modulation frequency; and $\phi$ is the modulation-phase angle difference between the angular velocity modulation and the potential modulation (Eq. 16). The importance of the modulation phase angle will be discussed later. Far from the RDE, there is no radial or azimuthal flow, that is

$$G(\tau, \infty) = F(\tau, \infty) = 0. \tag{6}$$

For our initial conditions, we take the fluid to be quiescent

$$G(0, \eta) = F(0, \eta) = H(0, \eta) = 0. \tag{7}$$

The governing equations and boundary conditions (Eqs. 3–7) are equivalent to the equations that govern fluid motion, when there is no deposition and the interface is defined by the plane $z^* = 0$ for all times. One can readily show that the translating frame modifies the pressure field, but does not affect the governing equations for $G$ and $F$.

### *Concentration field*

The dimensionless species continuity equation in the translating frame for a dilute, constant property electrolyte with negligible migration effects and no homogeneous reactions is (Newman, 1973)

$$\frac{\partial C_i}{\partial \tau} + H\frac{\partial C_i}{\partial \eta} = \frac{1}{Sc_i}\frac{\partial^2 C_i}{\partial \eta^2} \tag{8}$$

where $C_i(\tau, \eta) = c_i/c_{\infty i}$ is the dimensionless concentration of species $i$; $Sc_i = \nu/D_i$ is the Schmidt number; $D_i$ is the species $i$ diffusivity; and $c_{\infty i}$ is the bulk concentration of species $i$. Initially the concentration field is uniform

$$C_i(0, \eta) = 1, \tag{9}$$

and far from the RDE, the concentration takes on its bulk value

$$C_i(\tau, \infty) = 1. \tag{10}$$

At the electrolyte/deposit interface, the cation $M_i^{n_i+}$ is reduced to form deposit species $M_i^0$. The deposition reactions are of the form

$$M_i^{n_i+} + n_i e^- \rightleftharpoons M_i^0. \tag{11}$$

The electrode reactions proceed independently for each deposit species. We use a Butler-Volmer rate expression for each species $i$. The kinetic formulation is identical to that given by Verbrugge and Tobias (1985). The electrode kinetics in nondimensional form is

$$\frac{\partial C_i}{\partial \eta}(\tau, 0) = K_{c,i}(E)C_i(\tau, 0) - K_{a,i}(E)a_i, \tag{12}$$

where

$$K_{c,i} = \frac{k_{c,i}\sqrt{\nu/\Omega_o}\, e^{-\beta_i n_i f E}}{\rho_o D_i}, \tag{13}$$

and

$$K_{a,i} = \frac{k_{a,i}\sqrt{\nu/\Omega_o}\, e^{(1-\beta_i)n_i f E}}{c_{\infty i} D_i}, \tag{14}$$

are the dimensionless cathodic ($k_{c,i}$) and anodic ($k_{a,i}$) rate constants for species $i$. Here, $a_i$ is the solid state activity of species $i$ in the deposit; $\beta_i$ is the symmetry coefficient for the reaction of $i$; $n_i$ is the number of electrons transferred; $\rho_o$ is the solvent mass density; $E$ is the electrode potential relative to the normal hydrogen electrode (NHE) corrected for ohmic drop; and $f = F/RT$.

If the rate constants $K_{c,i}$ and $K_{a,i}$ are multiplied by $Sc^{-1/3}$, one can readily show that the resulting dimensionless groups $K_{c,i}Sc^{-1/3}$ and $K_{a,i}Sc^{-1/3}$ measure the relative importance of mass transfer resistance to kinetic resistance for the cathodic and anodic reactions, respectively. Since the factor $Sc^{-1/3}$ is proportional to the ratio of the concentration boundary layer thickness to the hydrodynamic boundary layer thickness, it follows that the quantity $\sqrt{\nu/\Omega_o}Sc^{-1/3}$ is the characteristic concentration boundary layer thickness. When $K_{c,i}Sc^{-1/3} \gg 1$ the reduction of species $i$ is mass-transfer-limited, whereas when $K_{c,i}Sc^{-1/3} \ll 1$ the reduction is activation-limited. The magnitude of $K_{a,i}Sc^{-1/3}$ determines the nature of the oxidation reaction of species $i$ in a similar way.

When the ohmic potential drop is negligible, the electrode potential can be written as (Verbrugge and Tobias, 1985)

$$E = V + U_{\text{ref}} \tag{15}$$

where $V$ is the measured potential difference between the RDE and the reference electrode and $U_{\text{ref}}$ is the potential difference between the reference electrode and a NHE. Equation 15 is used

later to convert kinetic parameters measured relative to a saturated calomel electrode (SCE) to a NHE basis. Otherwise, all potentials in this study will be referenced to a SCE. Formulations of the electrode potential that decompose $E$ into the sum of a surface overpotential and an open circuit potential also lead to kinetic expressions that are similar to Eq. 12 (White and Newman, 1977).

We consider a sinusoidal potential scheme that modulates the system at a single frequency. The instantaneous potential $V(\tau)$ is given by

$$V(\tau) = V_o + \Delta V \cos(p\tau) \tag{16}$$

where $V_o$ is the mean potential, and $\Delta V$ is the amplitude of the modulation potential. It follows from Eq. 16 that the dimensionless rate constants (Eqs. 13 and 14) are time-periodic. However, due to the exponential dependence of $K_{c,i}$ and $K_{a,i}$ on potential, the rate constants are not simple sinusoidal functions of time. We characterize the time-periodic modulation of $K_{c,i}$ and $K_{a,i}$ by defining

$$K^o_{c,i} = K_{c,i}(V_o), \tag{17}$$

and

$$\Delta K_{c,i} = K_{c,i}(V_o - \Delta V) - K_{c,i}(V_o + \Delta V). \tag{18}$$

Similar relationships hold for the dimensionless anodic rate constants. It is interesting to compare the angular velocity modulation waveform, Eq. 5, with the potential modulation waveform, Eq. 16. The angular velocity and potential are modulated at the same frequency $p$, but there is a phase angle difference $\phi$ between the angular velocity modulations and the potential modulations. We show later that changing $\phi$ can strongly affect the composition distribution in the electrodeposited alloy.

In this paper we use the term periodic plating to denote potential modulations of the form given by Eq. 16. The modulation frequencies considered here are $\sigma < 50$ Hz, so that charging currents are not deemed important (Puippe and Ibl, 1980). Although other potential modulation schemes can be used instead of Eq. 16, the simplicity of this equation allows us to more clearly isolate the effects of fluctuating flow on CMA electrodeposition.

Equations 3–10 and 12 were discretized using a Crank-Nicolson finite difference method. The computational algorithm used is described elsewhere (see Schwartz, 1989a). A minor modification to our previous code was necessary to account for the electrode kinetics. This was achieved by applying false boundary discretization to treat the flux condition (Eq. 12) at the electrode surface $\eta = 0$. The accuracy of the numerical computations was checked against approximate analytical solutions for the steady-state flux (Bard and Faulkner, 1980) and the time-periodic flux (Rosebrugh and Miller, 1910) induced by potential modulations of the form (Eq. 16). The deviations were less than 4% when large-amplitude, time-periodic potential modulations were used. This deviation is within the accuracy of Rosebrugh and Miller's approximate solution (Verbrugge and Tobias, 1985). Further details on the implementation and accuracy of the computational algorithm is given elsewhere (see Schwartz, 1989a).

The time-periodic results presented below were determined after the initial transients had decayed. The start-up time, denoted by $\tau_o = t_o\Omega_o$, necessary to achieve a steady periodic response was less than 90 radians for all cases studied. Calculations are presented for $\tau_o = 90$ radians.

At sufficiently low modulation frequencies ($p \ll Sc^{-1/3}$), the system response can be approximated as quasisteady. For $p \to 0$, the dimensionless concentration gradient of species $i$ at the RDE can be determined from the Levich equation (Miller and Bruckenstein, 1974)

$$\frac{\partial C_i}{\partial \eta}(\tau, 0) = \Gamma_i[\Omega(\tau)/\Omega_o]^{1/2}\{1 - C_i(\tau, 0)\}, \tag{19}$$

where $\Gamma_i = 0.620\, Sc_i^{1/3}$ for $Sc \gg 1$. $C_i(\tau, 0)$ can be eliminated from Eqs. 12 and 19 to get the quasisteady result

$$\frac{\partial C_i}{\partial \eta}(\tau, 0) = \Gamma_i\left[\frac{K_{c,i}(E) - K_{a,i}(E)a_i}{\Gamma_i[\Omega(\tau)/\Omega_o]^{1/2} + K_{c,i}(E)}\right]\left[\frac{\Omega(\tau)}{\Omega_o}\right]^{1/2}. \tag{20}$$

The time dependence in Eq. 20 arises from the angular velocity modulation given by Eq. 5, $\Omega(\tau)/\Omega_o$, and the potential modulation $E = E(\tau)$, given by Eqs. 15 and 16.

### *Alloy composition and growth*

The compositional make-up of the alloy can be calculated as a function of time once the concentration gradients for each species at the RDE are known. The mole fraction of species $i$ in a two-component alloy is given by

$$X_i(\tau) = \frac{\dfrac{\partial C_i}{\partial \eta}(\tau, 0)}{\displaystyle\sum_{k=1}^{2}\left[\frac{D_k c_{\infty k}}{D_i c_{\infty i}}\right]\frac{\partial C_k}{\partial \eta}(\tau, 0)}. \tag{21}$$

The quantity $D_k c_{\infty k}/D_i c_{\infty i}$ is what we referred to as the deposition ratio, since it equals the ratio of the mass-transfer-limited flux of species $k$ to the mass-transfer-limited flux of species $i$, when the Schmidt number for each species is identical. Note that the denominator in Eq. 21 is simply the sum of the dimensionless deposition rates of each species. The average composition of the alloy film at time $\tau'$ is determined by integrating the numerator of Eq. 21 from time $\tau = 0$ to time $\tau = \tau'$ and dividing that by the integral of the denominator of Eq. 21 over the same time period (from $\tau = 0$ to $\tau = \tau'$). The velocity of the deposit interface is

$$H^*_s(\tau) = v_s / \sqrt{\nu\Omega_o} = \sum_{k=1}^{2}\frac{m_k D_k c_{\infty k}}{\rho(\tau)\nu}\frac{\partial C_k}{\partial \eta}(\tau, 0) \tag{22}$$

where $\rho(\tau)$ is the deposit density, and $m_k$ is the atomic weight of species $k$. The time-periodic species $i$ flux has a dimensionless period of $T = 2\pi/p$. Integration of Eq. 22 over one modulation period yields the dimensionless modulation wavelength $\Lambda$

$$\Lambda = \frac{L}{\sqrt{\nu/\Omega_o}} = \int_{\tau_o}^{\tau_o+T}\sum_{k=1}^{2}\frac{m_k D_k c_{\infty k}}{\rho(\tau')\,\nu}\frac{\partial C_k}{\partial \eta}(\tau', 0)\, d\tau'. \tag{23}$$

Here $L$ denotes the thickness of the alloy unit cell. Although the derivation presented so far is for a two-component alloy, Eqs. 21–23 are readily generalized for $N$-component alloy.

The periodic region of the CMA consists of repeating unit cells. It is convenient to introduce a dimensionless variable for the alloy unit cell based on the periodicity wavelength $L$ so that the composition profile is defined in the domain $0 \le \zeta < 1$:

$$\zeta = \frac{z^* - z_o^*}{L} = \frac{\eta^* - \eta_o^*}{\Lambda}, \tag{24}$$

where the length $z_o^*$ is the thickness of the deposit at time $t_o$—an arbitrary time taken sufficiently large so that the system response is time-periodic.

## Electrochemical Kinetic Parameters

The most widely electroplated CMA has been Cu-Ni alloy (Tench and White, 1984; Yahalom and Zadok, 1987; Lashmore and Dariel, 1988). Copper, being the more noble metal (standard potential, $U^\theta = 0.340$ V for $Cu^{+2}/Cu$), plates at a more positive potential than does nickel (standard potential, $U^\theta = -0.23$ V for $Ni^{+2}/Ni$). Yahalom and Zadok (referred here as YZ) developed an electrolyte formulation, based on a 58°C Watts nickel bath, that has been used in numerous studies. The partial current density of $Ni^{+2}$ deposition, $i_{Ni}$, can be written as

$$-i_{Ni} = \left[\frac{nFD_{Ni}c_{\infty Ni}}{\sqrt{\nu/\Omega_o}}\right]\frac{\partial C_{Ni}}{\partial \eta}, \tag{25}$$

where we take cathodic currents to be negative. The reduction kinetics of $Ni^{+2}$ in YZ's electrolyte can be determined from the published data plotted in Figure 2 of YZ. The Tafel region for $Ni^{+2}$ deposition is given by the expression

$$-i_{Ni} = 1.07 \times 10^{-3}\, e^{-15.18V}\ (A/m^2), \tag{26}$$

where $V$ is in volts referenced to a SCE. The reaction order for $Ni^{+2}$ reduction is 1 in a standard Watts bath (Saraby-Reintjes and Fleischmann, 1984) and therefore the Butler-Volmer rate expression given by Eq. 12 is likely to hold for nickel deposition from the electrolyte formulation of YZ. The cathodic rate from Eq. 12 can be equated to Eq. 26, noting that Eq. 15 must also be applied, to obtain

$$1.07 \times 10^{-3}\, e^{15.18U_{ref}}\, e^{-15.18E} = n_{Ni}F\,\frac{k_{c,Ni}c_{Ni}(t,0)}{\rho_o}\, e^{-\beta_{Ni}n_{Ni}fE}. \tag{27}$$

The above result can be rearranged to find that $\beta_{Ni}n_{Ni}f = 15.18$ holds for YZ's electrolyte, and that

$$k_{c,Ni} = \frac{1.07 \times 10^{-3}\, e^{15.18U_{ref}}\,\rho_o}{n_{Ni}F\,c_{Ni}(t,0)}. \tag{28}$$

The concentration of $Ni^{+2}$ at the electrode surface will be nearly identical to the bulk concentration since the kinetics are determined from the Tafel region; hence, $c_{Ni}(t, 0) \approx 1.44 \times 10^3$ mol/m$^3$. At 58°C, the potential difference between SCE and NHE reference electrodes is $U_{ref} \approx 0.2174$ V (Bard and Faulkner, 1980). The density of the electrolyte is estimated to be $\rho_o \approx 10^3$ kg/m$^3$, and the number of electrons transferred for $Ni^{+2}$ reduction is $n_{Ni} = 2$. Given these parameters, the cathodic rate constant for Ni deposition in YZ's bath is estimated from Eq. 28 to be $k_{c,Ni} = 1.04 \times 10^{-7}$ kg/m$^2$ · s. The other kinetic parameters in YZ's electrolyte cannot be determined explicitly from the data they provide. Order of magnitude estimates, however, can be made from YZ's data to determine the relative importance of the kinetic terms in Eq. 12 for each species $i$.

In order to evaluate the dimensionless kinetic parameters $K_{c,i}$ and $K_{a,i}$ for YZ's bath, it is necessary to determine some additional physical properties of the electrolyte. The electrolyte kinematic viscosity is taken to be $\nu = 10^{-6}$ m$^2$/s; the species diffusivities are estimated to be $D_i = 10^{-9}$ m$^2$/s; and the deposit density is estimated to be $\rho = 8.5 \times 10^3$ kg/m$^3$. The following parameters have known values or are given by YZ: $m_{Ni} = 0.0587$ kg/mol; $m_{Cu} = 0.06355$ kg/mol; $c_{\infty Cu} = 2.8$ mol/m$^3$; and $c_{\infty Ni} = 1.44 \times 10^3$ mol/m$^3$. For our analysis, we take $\Omega_o = 1{,}600$ rpm so that the possibility of natural convection need not be considered when the disk has slowed to its minimum angular velocity during a modulation period when $\alpha = 0.9$. (See Eq. 5.) Using the above parameters, we find that $K_{c,Ni}$ is given by

$$K_{c,Ni} = 2.97 \times 10^{-7}\, e^{-15.18V}, \tag{29}$$

where $V$ is referenced to a SCE. The Schmidt number for this system is 1,000. Thus, $K_{c,Ni}Sc^{-1/3} = 1$ when $V = -1.142$ V vs. SCE. Recall that Ni deposition is activation-limited when $K_{c,Ni}Sc^{-1/3} \ll 1$, and Ni deposition is mass-transfer-limited when $K_{c,Ni}Sc^{-1/3} \gg 1$. YZ's data show that mass transfer effects become increasingly important for Ni deposition at potentials more negative than $-1.0$ V vs. SCE (i.e., $K_{c,Ni}Sc^{-1/3} > 0.12$).

We restrict the potential range of interest to $-1.0 \le V \le -0.3$ V vs. SCE ($2.82 \times 10^{-5} \le K_{c,Ni} \le 1.16$) in order to consider operating conditions similar to those of YZ. Yahalom and Zadok found that the current efficiency was greater than 90% when the potential was positive of $-1.0$ V, indicating that the hydrogen evolution reaction can be taken as negligible in this system. From Figure 2 of YZ, one can also estimate the magnitudes of $K_{a,Ni}$, $K_{c,Cu}$, and $K_{a,Cu}$, but not the absolute values. For potentials more negative than $-0.3$ V vs. SCE, YZ's data show that the anodic dissolution for both Ni and Cu are negligible and that the cathodic deposition of Cu is mass-transfer-limited. Thus, YZ's data suggest the following: $K_{a,Ni}Sc^{-1/3} \ll 1$; $K_{a,Cu}Sc^{-1/3} \ll 1$; and $K_{c,Cu}Sc^{-1/3} \gg 1$.

In all of our computations, both anodic rate parameters are set to zero, i.e., $K_{a,Ni} = K_{a,Cu} = 0$, and the Cu cathodic rate parameter is set sufficiently large so that mass transfer is the limiting rate, i.e., $K_{c,Cu}Sc^{-1/3} \gg 1$. The dimensionless Ni kinetic rate parameter is given by Eq. 29.

It is well known that the current distribution of an activation-limited species, such as Ni, can have substantial radial nonuniformity at a RDE, resulting in CMA's with spatial varying thicknesses and compositions. For some thin-film applications, layer nonuniformity may limit the usefulness of electrodeposited CMA's (Slonczewski et al., 1988). Using the properties of the electrolyte described above, as well as estimates for the electrolyte conductivity and the $Ni^{+2}$ transference number, we estimate that the dimensionless groups $N$, $\delta$, and $J$ derived by Newman (1973) to describe radial nonuniformity are $O(1)$, $O(1)$, and $\ll 1$, respectively. This implies that the deposit is uniform under the conditions given above (Newman, 1973; section 132).

The formulation as presented here is in terms of dimension-

less variables and therefore is valid for other alloy pairs that satisfy the constraints laid out above. Cu-Ni deposition data are used throughout this paper in order to assure that the parameters employed are physically realizable.

## Results

The $z$ direction in the deposit is normal to the planes of uniform composition and the electrode surface. Since we will be considering the spatially-periodic region of the alloy, it is convenient to use the unit cell variable $\zeta = (z^* - z_o^*)/L$ in our discussion so that all of the alloy characterisitcs are represented by $0 \leq \zeta < 1$ (Eq. 24). If we consider the light regions in Figure 1a to be rich in species 1 and the dark regions to be rich in species 2, then the curve drawn in Figure 1b is a representation of the alloy mole fraction $X_1$ as a function of the unit cell position $\zeta$.

The mole fraction profile shown in Figure 1b has a number of features that are useful for quantifying the characteristics of the compositional distribution of the alloy. Asymmetry in the composition profile can be gauged by comparing the maximum positive mole fraction gradient, SLOPE 1 = max $\{\partial X_1/\partial\zeta\}$, to the minimum negative mole fraction gradient, SLOPE 2 = min $\{\partial X_1/\partial\zeta\}$. A necessary condition, though obviously not sufficient, for the alloy to be symmetric is that SLOPE 1 equals the absolute value of SLOPE 2. The total mole fraction variation over the unit cell is given by $\Delta X_1$. The full width at half maximum (*fwhm*) of the alloy composition modulation is a measure of the thickness of the layer rich in species 1. Since the results reported here are based on the kinetics of Cu-Ni deposition, we will denote species 1 to be copper and species 2 to be nickel. Thus, *fwhm* indicates the fraction of the alloy unit cell consisting of a copper-rich layer or, in other words, the relative thickness of the copper-rich band.

CMA's can form when the flow, potential or both are modulated. In order to understand the effects of flow on the formation of pulse-plated CMA's, we consider first the cases of flow-induced CMA's and potential-induced CMA's. We then consider the more complicated situation, where the CMA is plated in a fluctuating flow with periodic potential modulations.

### *Fluctuating flow ($\alpha$ = 0.9) with a fixed potential*

The Cu mole fraction profiles shown in Figure 2a represent Cu-Ni CMA induced solely by fluctuating flow. The set of curves in Figure 2b are plots of the composition gradients for the three profiles shown in Figure 2a. The angular velocity of the RDE is modulated with amplitude of $\alpha = 0.9$ and frequency $p = 0.01$ (Eq. 5). Curve 1 in Figure 2 corresponds to deposition with $K^o_{c,Ni} = 0.00268$ ($V_o = -0.6$ V vs. SCE). Curves 2 and 3 correspond to $K^o_{c,Ni} = 0.0122$ and $K^o_{c,Ni} = 0.0558$ ($V_o = -0.7$ and $-0.8$ V, respectively). $\Delta K_{c,Ni}$ is zero for all three curves. The composition distributions are the result of time-periodic variations in the deposition rate of Cu due to the fluctuating flow induced by the speed-modulated RDE (recall $K^o_{c,Cu} Sc^{-1/3} \gg 1$). The Ni deposition rate for each curve in Figure 2 is essentially constant since $\Delta K_{c,Ni} = 0$ and $K^o_{c,Ni} Sc^{-1/3} \ll 1$.

The asymmetry that is present in flow-induced CMA's is clearly evident in Figure 2b. The compositional gradients are considerably larger around $\zeta \approx 0.1$ than near $\zeta \approx 0.9$. Asymmetry arises from the nonlinearity present in the governing equations, and the time dependence of $H$ in Eq. 8. Schwartz et al. (1989) have shown that large angular velocity modulation amplitudes, i.e., $\alpha \sim O(1)$, lead to higher harmonic response in the flux to a speed-modulated RDE. (See also Appendix A.) Phase lag present in the higher harmonics tends to skew the $Cu^{+2}$ flux at the RDE. As $\alpha \to 0$, our calculations confirm that the flux of $Cu^{+2}$ becomes symmetric due to the suppression of higher harmonic components in the flux, and fluctuations in the allow composition approach zero.

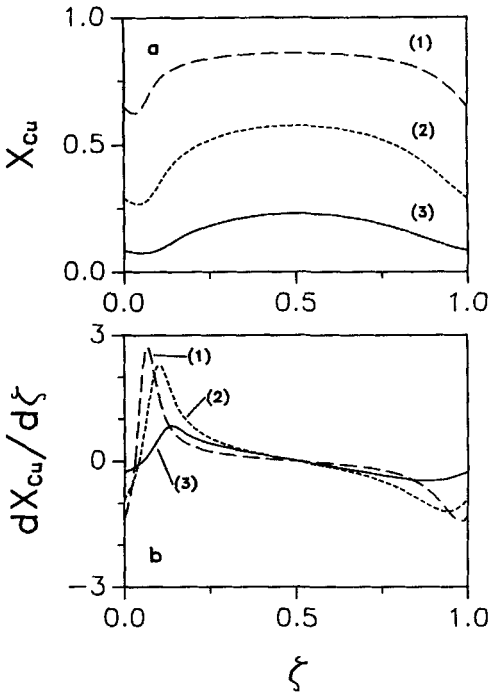


**Figure 2. Computed alloy composition profiles for Cu-Ni CMA's induced by fluctuating flow.**

(a) Cu mole fraction profiles.

(b) Mole fraction gradient profiles: 1) $K^o_{c,Ni} = 0.00268$ ($L = 7.0$ nm); 2) $K^o_{c,Ni} = 0.0122$ ($L = 11.5$ nm); 3) $K^o_{c,Ni} = 0.0558$ ($L = 31.7$ nm); $\Delta K_{c,Ni} = 0$, $\alpha = 0.9$; and $p = 0.01$. The values $Sc_i = 1{,}000$ and $D_{Ni}c_{\infty Ni}/D_{Cu}c_{\infty Cu} = 514.3$ are identical for all the figures.

Plotted in Figure 3 are the quantities that characterize the composition distribution of a CMA unit cell as a function of the rate parameter for the activation-limited species, $K^o_{c,Ni}$. The definitions for $\Delta X_{Cu}$, *fwhm*, SLOPE 1, and SLOPE 2 are given in Figure 1b. The mean alloy composition $\bar{X}_{Cu}$, plotted in Figure 3b, is defined as

$$\bar{X}_{Cu} = \int_0^1 X_{Cu}(\zeta)\, d\zeta. \tag{30}$$

The total mole fraction variation in the alloy, $\Delta X_{Cu}$, is plotted vs. $K^o_{c,Ni}$ for the range $0.000588 \leq K^o_{c,Ni} \leq 0.255$ ($-0.9 \leq V_o \leq -0.5$ V vs. SCE). A maximum in $\Delta X_{Cu}$ is seen in Figure 3a when $K^o_{c,Ni}$ is between 0.00573 and 0.0122 ($V_o$ is between $-0.7$ and $-0.65$ V). The maximum in $\Delta X_{Cu}$ occurs when the average deposition rates of Cu and Ni are nearly identical at the RDE surface (Schwartz, 1989b). For the conditions used here, the deposition rate of each species is equal when $K^o_{c,Ni} \approx 0.01$ ($V_o \approx -0.69$ V). This can be deduced from Figure 3b by noting that $\bar{X}_{Cu} \approx 0.5$ when $K^o_{c,Ni} \approx 0.01$. Clearly, changing the transport properties of the electrolyte, as measured by the Schmidt number and the deposition ratio, will modify the value of $K^o_{c,Ni}$ that

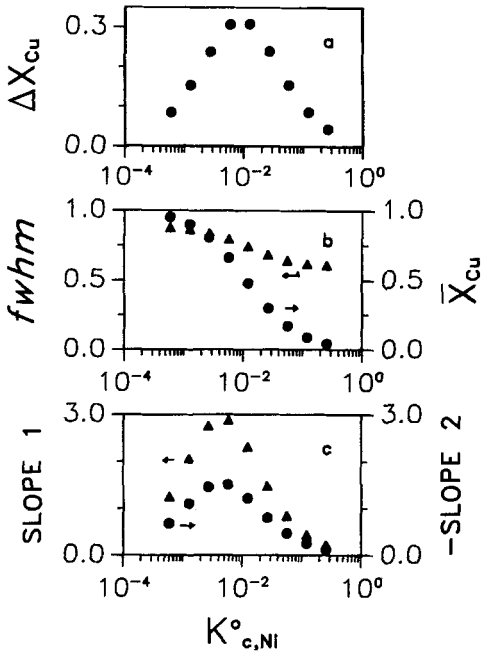


**Figure 3. Dependence of unit cell characteristics for a flow-induced CMA on the kinetic parameter $K^o_{c,Ni}$.**

(a) Total unit cell mole fraction variation.
(b) *fwhm* and spatially-averaged alloy composition
(c) Maximum positive and negative mole fraction gradients; $\Delta K_{c,Ni} = 0$, $\alpha = 0.9$, and $p = 0.01$.

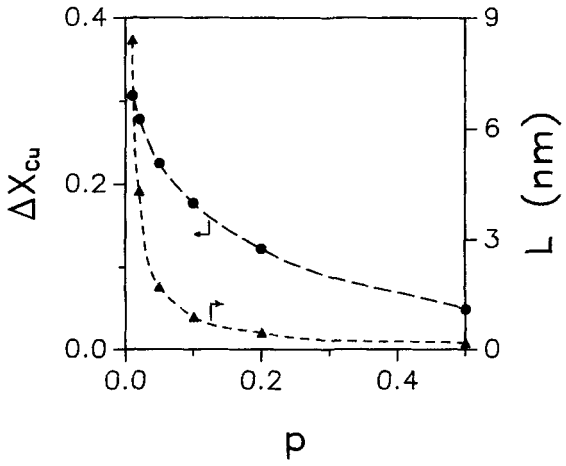


**Figure 4. Frequency dependence of the total unit cell mole fraction variation and the alloy periodicity wavelength for a flow-induced CMA.**

$K^o_{c,Ni} = 0.00573$; $\Delta K_{c,Ni} = 0$; and $\alpha = 0.9$.

gives equal Cu and Ni deposition rates. (See the discussion following Eq. 21.)

Plotted in Figure 3b is the unit cell thickness of the Cu-rich region (*fwhm*) and the average alloy composition ($\bar{X}_{Cu}$) as a function of $K^o_{c,Ni}$. The thickness of the Cu-rich layer is seen to decrease continuously as $K^o_{c,Ni}$ increases. Increasing $K^o_{c,Ni}$ increases the Ni deposition rate, and the alloy goes from being nearly-pure Cu to nearly-pure Ni.

SLOPE 1 and -SLOPE 2 are plotted in Figure 3c as a function of the kinetic parameter $K^o_{c,Ni}$. The two slopes are not equal but both slopes rise to a maximum near $K^o_{c,Ni} \approx 0.006$. The maxima occur at a $K^o_{c,Ni}$ value where the average Cu deposition rate is slightly greater than the Ni deposition rate.

In Figure 4 we examine the effect of the modulation frequency on alloy composition and the unit cell wavelength $L$. It is well known that fluctuations in the flux induced by a speed modulated RDE are attenuated as the modulation frequency $p$ increases (Schwartz et al., 1989; Tribollet and Newman, 1983). This arises from mass transfer and hydrodynamic relaxation time scales. The mass transfer relaxation time is on the order of $Sc^{-1/3}$ in electrochemical systems whereas the hydrodynamic time scale is on the order of 1 (Tribollet and Newman, 1983). Because of the disparity in the time scales, smaller Schmidt numbers lead to faster mass transfer response and less attenuation of the modulation effect in the alloy as frequency increases (Schwartz, 1989b). In addition, when $p$ increases, the modulation period decreases and less alloy is deposited during each modulation cycle, resulting in a decrease in the unit cell wavelength $L$. These effects are illustrated in Figure 4.

The aforementioned results show that fluctuating flow alone is able to produce short wavelength Cu-Ni CMAs if $K^o_{c,Ni}$ is roughly within the range $0.0006 < K^o_{c,Ni} < 0.25$ ($-0.9 < V_o < -0.5$ V vs. SCE for Cu-Ni kinetics), $K^o_{c,Cu}Sc^{-1/3}$ is much larger than 1, and the modulation frequency is $p \leq 0.5$ for $\alpha = 0.9$ and $Sc = 1{,}000$. These results hold for other alloy pairs with similar rate parameters, Schmidt numbers, and bath compositions. When $K^o_c$ values for the activation-limited species are outside the range presented here, the plated alloy will not be strongly affected by fluctuations in the flow field because the deposit will be essentially pure Cu ($K^o_{c,Ni} < 0.0006$) or pure Ni ($K^o_{c,Ni} > 0.25$). Electrodeposition with $K^o_{c,Ni} \approx 0.01$ tends to maximize the total mole fraction variation and the composition gradients in the unit cell. This is because the deposition rates of both species are nearly identical when $K^o_{c,Ni} \approx 0.01$. Of course, when the amplitude of the flow fluctuations are small ($\alpha \ll 1$), significant flow-induced CMA's will not form.

### *Periodic potential modulations with steady flow ($\alpha = 0$)*

We consider the effect of potential modulations given by Eq. 16 on the plating of CMA's when the RDE is rotating at a steady angular velocity $\Omega_o$ ($\alpha = 0$). Although all the results reported in this section are numerical, it should be noted that analytical solutions to the transient species continuity equation and its boundary conditions (Eqs. 8–12) can be found when $\alpha = 0$ (Verbrugge and Tobias, 1985), or when $\alpha \ll 1$ (Deslouis et al., 1983).

We first examine the effect of changing the potential modulation amplitude $\Delta V$ on the spatial distribution of Cu in the unit cell. As previously noted, modulating the potential causes all of the kinetic rate parameters to be time-periodic. Recall that we characterize the periodic modulations in the cathodic rate parameter $K_{c,i}$ by defining $\Delta K_{c,i} = K_{c,i}(V_o - \Delta V) - K_{c,i}(V_o + \Delta V)$. The only kinetic parameter that influences the deposition process for the Cu-Ni system studied here is $K_{c,Ni}$, since all of the other rate parameters are either very large or very small compared to unity. The time-periodic nature of $K_{c,Ni}$ induces a time-periodic deposition rate for Ni. The Cu deposition rate is constant since the angular velocity of the RDE is fixed ($\alpha = 0$) and $K_{c,Cu}Sc^{-1/3} \gg 1$. It is interesting to note that $\Delta K_{c,Ni}$ will often be larger than $K^o_{c,Ni}$, but this does not mean that $K_{c,Ni}$ becomes nega-

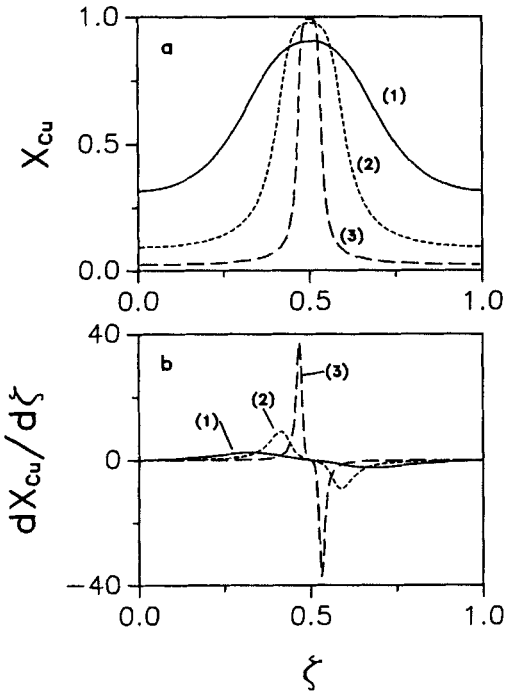


**Figure 5. Computed alloy composition profiles for Cu-Ni CMA's induced by three different potential modulation amplitudes ($V_o = -0.65$ V).**

(a) Cu mole fraction profiles.

(b) Mole fraction gradient profiles: 1) $\Delta K_{c,Ni} = 0.0249$ ($\Delta V = 0.1$ V, $L = 10.6$ nm); 2) $\Delta K_{c,Ni} = 0.119$ ($\Delta V = 0.2$ V, $L = 19.5$ nm; 3) $\Delta K_{c,Ni} = 0.544$ ($\Delta V = 0.3$ V, $L = 52.6$ nm); $K^o_{c,Ni} = 0.00573$, $\alpha = 0$, and $p = 0.01$.

tive during each modulation period. In fact, Eq. 29 shows that $K_{c,Ni}$ is positive and has an exponential dependence on potential that causes $K_{c,Ni}$ to increase rapidly as the electrode potential becomes more negative. For example, when $V_o = -0.65$ V and $\Delta V = 0.3$, Eq. 29 yields $K_{c,Ni}(V_o - \Delta V) = 0.54415$, and $K_{c,Ni}(V_o + \Delta V) = 0.00006$. Thus, $\Delta K_{c,Ni} = 0.54409$ and is large compared to $K^o_{c,Ni}$. It is the exponential potential dependence of $K_{c,Ni}$ that gives rise to higher harmonic response in the time-periodic $Ni^{+2}$ flux. (Further details are given in Appendix A.) Moreover, it is expected that the exponential dependence of $K_{c,Ni}$ on potential will induce large mole fraction gradients in the CMA.

CMA's induced by the potential modulation scheme (Eq. 16) are shown in Figure 5 to be nearly symmetric. There are no relaxation time scales associated with the Ni deposition reaction since convective-diffusive effects are small ($K_{c,Ni}Sc^{-1/3} \ll 1$), as are interfacial capacitive effects due to the low frequencies employed here (Puippe and Ibl, 1980). In other words, the Ni deposition reaction responds nearly instantaneously to perturbations in the electrode potential, at least for the range of parameters explored in this study. Therefore, the symmetry observed in figure 5 occurs because the Ni deposition kinetics act as a purely resistive, though nonlinear (in the sense of admittance studies), element in the ac response of this system. If values of $K^o_{c,Ni}Sc^{-1/3}$ greater than approximately 0.1 ($V \approx -1.0$ V vs. SCE) are included in the potential modulation cycle, mass transfer relaxation effects will tend to skew the Ni flux waveform, resulting in an asymmetric alloy profile. Skewing associated with mass transfer time scales is observed in the pulse plating work of Verbrugge and Tobias (1985) and Ruffoni and Landolt (1988).

The large mole fraction gradients that arise when $\Delta K_{c,Ni} = 0.544$ ($\Delta V = 0.3$ V) are a result of the exponential potential dependence of the Butler-Volmer kinetics (Eqs. 12–14), as discussed above. When $\Delta K_{c,Ni}$ approaches zero, the Ni deposition rate fluctuates at a single frequency that causes the spatial Cu profile to vary sinusoidally. This effect is evident in Figure 5a for $\Delta K_{c,Ni} = 0.0249$ ($\Delta V = 0.1$ V). It is interesting to note that the periodicity wavelength *increases* from $L = 10.6$ nm when $\Delta K_{c,Ni} = 0.0249$ to $L = 52.6$ nm when $\Delta K_{c,Ni} = 0.544$, even though $K^o_{c,Ni}$ is held fixed. Figures 5a and 5b also show that the total Cu composition variation $\Delta X_{Cu}$ and the maximum gradients increase as $\Delta K_{c,Ni}$ increases.

Figure 6 shows the effect of the mean potential (measured by the rate parameter $K^o_{c,Ni}$) on the composition profile of a Cu-Ni CMA when the potential modulation amplitude is $\Delta V = 0.3$ V. Three major trends are observed when $K^o_{c,Ni}$ is changed from $K^o_{c,Ni} = 0.00268$ to $K^o_{c,Ni} = 0.0122$: the thickness of the Cu-rich layer (*fwhm*) decreases, the composition gradients become larger, and as noted in the caption the periodicity wavelength increases. The results shown in Figure 6 suggest that the alloy becomes nearly-pure Ni as $K^o_{c,Ni}$ increases. Conversely, the alloy will become nearly-pure Cu as $K^o_{c,Ni}$ decreases (anodic dissolution of the deposit must also be accounted for as $V_o$ becomes more positive than 0.3 V vs. SCE). Because of the form of Eq. 29, one can show that changing $K^o_{c,Ni}$ also changes $\Delta K_{c,Ni}$, even though $\Delta V$ is held constant. These changes are noted in Figure 6.

From the data on wavelength given in Figures 5 and 6, we

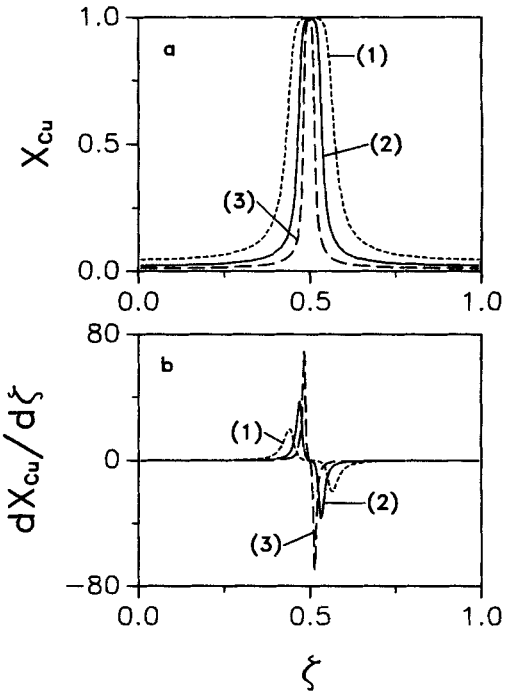


**Figure 6. Computed alloy composition profiles for Cu-Ni CMA's induced by periodic potential modulations with three different mean potentials ($\Delta V = 0.03$ V).**

(a) Cu mole fraction profiles.

(b) Mole fraction gradient profiles: 1) $K^o_{c,Ni} = 0.00268$; $\Delta K_{c,Ni} = 0.255$ ($V_o = -0.6$ V, $L = 28.6$ nm); 2) $K^o_{c,Ni} = 0.00573$, $\Delta K_{c,Ni} = 0.544$ ($V_o = -0.65$ V, $L = 52.6$ nm); 3) $K^o_{c,Ni} = 0.0122$, $K_{c,Ni} = 1.16$ ($V_o = -0.7$ V, $L = 99.5$ nm); $\alpha = 0$, and $p = 0.01$.

observe that any variation in the kinetic parameters ($K^o_{c,Ni}$ or $\Delta K_{c,Ni}$) that enhances the average deposition rate of Ni also increases the periodicity wavelength of the alloy when potential modulations of the form Eq. 16 are used. The periodicity wavelength is determined from the sum of the deposition rates for each alloy species, integrated over a single modulation period (Eq. 23). The Cu deposition rate is constant, so increasing the average Ni deposition rate provides an attendant increase in $L$. It is clear that there is an interdependence among the unit cell composition, wavelength, and composition gradients, and that variations in kinetic or transport parameters will modify the unit cell characteristics in a complex fashion.

### *Simultaneous fluctuating flow ($\alpha$ = 0.9) and periodic potential modulations*

The preceding sections have shown that fluctuating flow can induce Cu-Ni CMA's, but that periodic potential modulations can provide a much more dramatic modulation effect in the alloy. Given this, one may expect that fluctuating flow will only slightly perturb the composition profile of a pulse-plated CMA. In this section we show that fluctuating flow can significantly modify the unit cell characteristics of a plated CMA and, moreover, the influence of fluctuating flow is very sensitive to the modulation-phase-angle difference $\phi$ between the potential and the angular velocity waveforms (cf. Eqs. 5 and 16).

In Figures 7 and 8, composition and composition gradient profiles are plotted for values of $\phi$ that emphasize the influence of the modulation phase difference. In Figure 7, we show unit

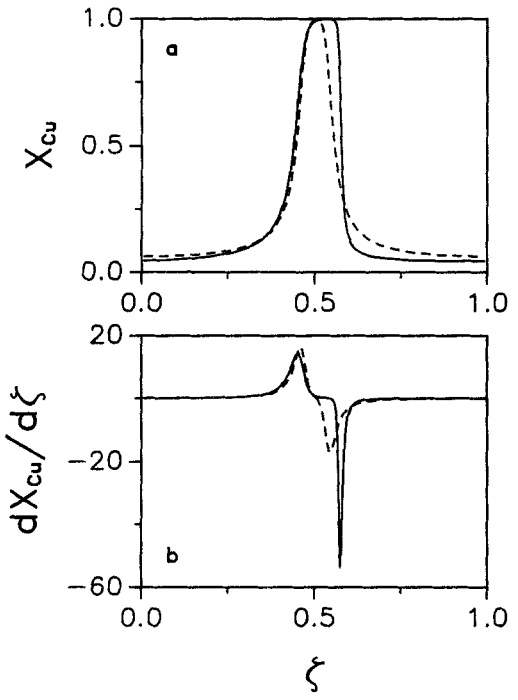


**Figure 7. Alloy composition profiles for Cu-Ni CMA's electrodeposited in fluctuating flow with simultaneous periodic potential modulations at a frequency of $p$ = 0.01 ($V_o$ = −0.6 V, $\Delta V$ = 0.3 V).**

(a) Cu mole fraction profiles.
(b) Mole fraction gradient profiles.
Dashed lines, $\phi$ = 0° ($L$ = 28.4 nm); solid lines, $\phi$ = 90° ($L$ = 28.2 nm); $K_{c,Ni}$ = 0.00268, $\Delta K_{c,Ni}$ = 0.255, $\alpha$ = 0.9, and $p$ = 0.01.

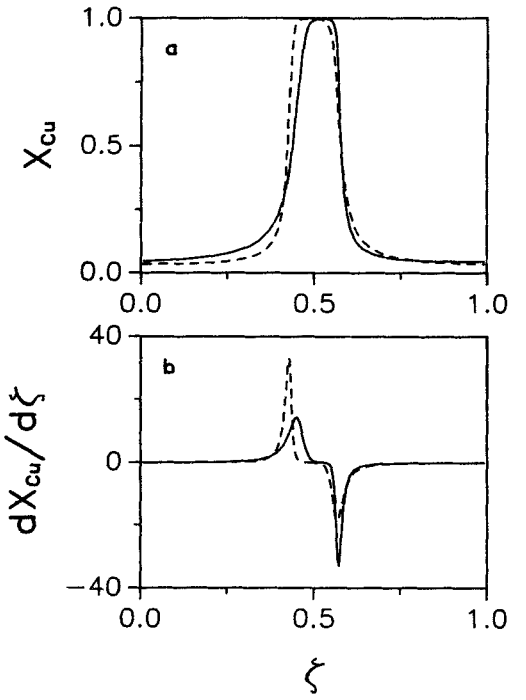


**Figure 8. Alloy composition profiles for Cu-Ni CMA's electrodeposited in fluctuating flow with simultaneous periodic potential modulations at a frequency of $p$ = 0.1 ($V_o$ = −0.6 V, $\Delta V$ = 0.3 V).**

(a) Cu mole fraction profiles.
(b) Mole fraction gradient profiles.
Dashed lines, $\phi$ = 180° ($L$ = 2.9 nm); solid lines, $\phi$ = 45° ($L$ = 2.9 nm); $K_{c,Ni}$ = 0.00268, $\Delta K_{c,Ni}$ = 0.255, $\alpha$ = 0.9, and $p$ = 0.01.

cell profiles for $\phi$ = 0° and 90° when $p$ = 0.01, and in Figure 8 profiles for $\phi$ = 45° and 180° when $p$ = 0.1. The kinetic and mass transfer parameters are held fixed ($K^o_{c,Ni}$ = 0.00268; $\Delta K_{c,Ni}$ = 0.255; $\alpha$ = 0.9; $Sc$ = 1,000; and $c_{\infty 2}/c_{\infty 1}$ = 514.3). Many of the unit cell features, such as $\Delta X_{Cu}$, $\bar{X}_{Cu}$, and *fwhm*, that can be deduced from Figures 7 and 8 are determined to a large degree by the characteristics of the potential waveform and are not affected too greatly by $\phi$. Indeed, if one is interested only in $\Delta X_{Cu}$ or *fwhm*, then the presence of fluctuating flow does not change the deposition process significantly. Figure 7, however, does shows that flow modulations can modify the symmetry and interphase gradients in a plated CMA. By changing the modulation phase angle from $\phi$ = 0° to $\phi$ = 90°, one observes that the alloy profile becomes rather asymmetric. The asymmetry in the unit cell is quantified in Figure 7b where we show that changing $\phi$ more than triples the mole fraction gradient in the interphase region located at $\zeta > 0.5$. Although these effects are also present when $p$ = 0.1 (Figure 8), the effect of the modulation phase angle on the alloy composition distribution is reduced as frequency increases (cf. Figure 7). The reason for this is discussed in the next section.

Figure 9 shows the effect of the modulation frequency $p$ on the unit cell composition profiles for two alloys plated under identical conditions. The alloy plated at a "high" frequency ($p$ = 1, solid line) is symmetric and has a nondimensional unit cell that is nearly identical to curve 1 in Figure 6. Though not shown, changing $\phi$ does not effect the composition distribution of the alloy deposited at $p$ = 1, and therefore fluctuating flow

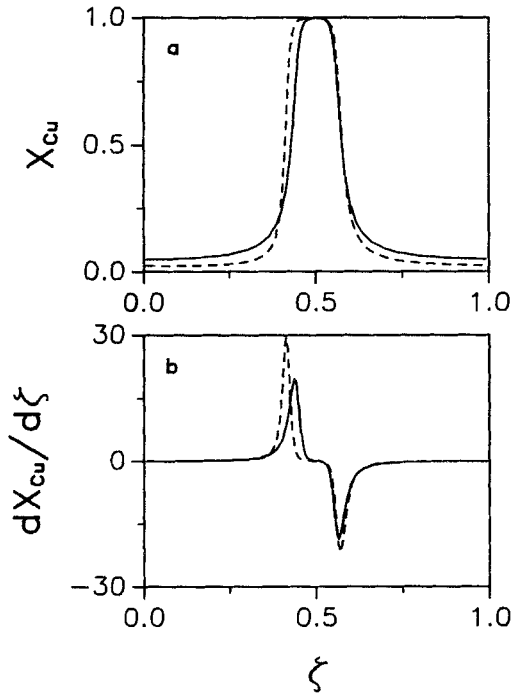


**Figure 9. Alloy composition profiles for Cu-Ni CMA's electrodeposited in fluctuating flow with simultaneous potential modulations ($V_o$ = −0.6 V, $\Delta V$ = 0.3 V).**

(a) Cu mole fraction profiles.
(b) Mole fraction gradient profiles.
Dashed lines, $p$ = 0.02 ($L$ = 14.0 nm); solid lines, $p$ = 1 ($L$ = 0.3 nm); $K^o_{c,Ni}$ = 0.00268, $\Delta K_{c,Ni}$ = 0.255, $\alpha$ = 0.9, and $\phi$ = 180°.

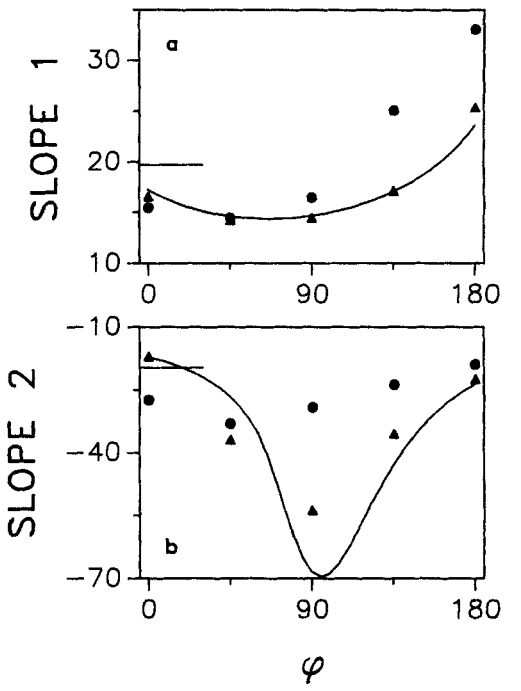


**Figure 10. Modulation phase angle dependence of SLOPE 1 and SLOPE 2 for $p \to 0$ (—), $p$ = 0.01 (Δ), and $p$ = 0.1 (O).**

$K^o_{c,Ni}$ = 0.00268; $\Delta K_{c,Ni}$ = 0.255; and $\alpha$ = 0.9.
The horizontal line on the left of each plot is the value for steady flow, $\alpha$ = 0.

has negligible influence on the deposition process at that frequency. The alloy plated at a "low" frequency ($p$ = 0.02, dashed line) is asymmetric and is similar to the alloys represented in Figure 7. Note that, in dimensional terms, the unit cells for the $p$ = 0.02 curve ($L$ = 14.0 nm) and the $p$ = 1 curve in Figure 9 ($L$ = 0.3 nm) are quite different since they are formed at different modulation frequencies. Nondimensionalization of the alloy unit cell based on the material periodicity wavelength, Eq. 24, provides a rational basis for comparing the composition distributions of these very different alloys.

## Mass Transfer Relaxation Effects

When the flow is steady ($\alpha$ = 0), the composition of the CMA is symmetric within the unit cell (cf. Figure 5), and the mole fraction gradients SLOPE 1 and SLOPE 2 are identical. We have seen from Figures 7 and 8 that the modulation phase angle $\phi$ between the fluctuating flow and the periodic potential can have a significant effect on the composition distribution in the CMA. We pursue this aspect further by examining the dependence of $\Delta X_{Cu}$, *fwhm*, SLOPE 1 and SLOPE 2 on both $\phi$ and $p$. In Figures 10 and 11, three sets of data, each for a different modulation frequency $p$ are plotted against $\phi$ for $K^o_{c,Ni}$ = 0.00268, $\Delta K_{c,Ni}$ = 0.255, $\alpha$ = 0.9, $Sc$ = 1,000, and $c_{\infty 2}/c_{\infty 1}$ = 514.3. The solid curve denotes the quasisteady limit ($p \to 0$), given by Eq. 20. The horizontal line on the lefthand side of each graph corresponds to the value of the dependent variable when the flow is steady, i.e., $\alpha$ = 0.

Figure 10 shows the influence of the fluctuating flow on the Cu-Ni interphase mole fraction gradients, as measured by SLOPE 1 and SLOPE 2. In the quasisteady limit, the largest mole fraction gradient that is achieved (given by SLOPE 2) has a magnitude of 70 at $\phi \approx 95°$. The magnitude of SLOPE 2 decreases to 54 near $\phi \approx 90°$ when $p$ = 0.01 and to 33 near $\phi \approx 45°$ when $p$ = 0.1. These results confirm our previous statement that flow effects become less important at higher frequencies.

Figure 11 shows that neither $\Delta X_{Cu}$ nor *fwhm* changes as dramatically as do the interphase composition gradients (plotted in Figure 10) when $\phi$ is varied, since $\Delta X_{Cu}$ and *fwhm* are determined primarily by the kinetic parameters $K^o_{c,Ni}$ and $\Delta K_{c,Ni}$, rather than by the flow conditions. This is borne out in Figure 11.

It is useful to determine the frequency range where fluctuating flow will affect the CMA deposition process and where the effects are diminished. Figure 4 shows that mass transfer relaxation is responsible for reducing the effects of fluctuating flow as frequency increases. It is well known in the electrochemical literature that the flux response to small-amplitude flow fluctuations ($\alpha \ll 1$) has a characteristic mass transfer relaxation time that scales as $O(Sc^{-1/3})$ (Tribollet and Newman, 1983). The flux response to large-amplitude flow fluctuations [$\alpha \sim O(1)$] shows similar trends (Schwartz et al., 1989). A characteristic frequency for mass transfer relaxation ($p_c$) is the reciprocal of the mass transfer time scale, or $p_c \sim O(Sc^{-1/3})$. Thus, fluctuating flow is expected to modify periodically-plated CMA's when $p \ll p_c$, where $p_c$ is based on the Schmidt number of the most noble alloy component, and fluctuating flow will have negligible effect when $p \gg p_c$. For the Cu-Ni system analyzed here, $p_c \sim 0.01$. In Figure 4 we see that $\Delta X_{Cu}$ decreases rapidly above a fre-

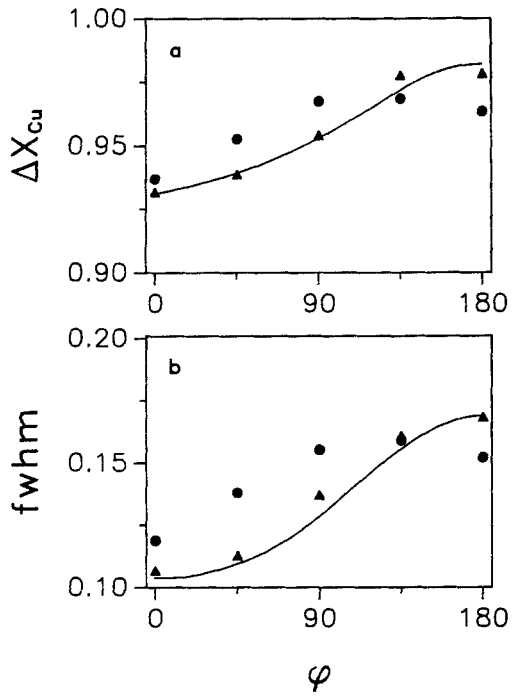


**Figure 11. Modulation phase angle dependence of $\Delta X_{Cu}$ and *fwhm* for $p \to 0$ (—), $p = 0.01$ (Δ), and $p = 0.1$ (O).**

$K^{\circ}_{c,Ni} = 0.00268$, $\Delta K_{c,Ni} = 0.255$, and $\alpha = 0.9$.

quency of $p \approx 0.1$. Figures 7 through 11 show also that the effect of fluctuating flow is diminished when the frequency is $O(p_c)$ or greater.

## Concluding Remarks

We report results from a theoretical investigation aimed at analyzing the effects of fluctuating flow on the composition distribution in electrodeposited composition modulated alloys. Kinetic and transport parameters are obtained from the experimental literature on Cu-Ni alloy electrodeposition. Fluctuating flow is shown to substantially alter the composition distribution of alloys plated with periodic potential modulations, especially within the interphase region of the unit cell where composition gradients are the greatest. Our results show that asymmetric alloys are often formed when fluctuating flow effects are taken into account. The asymmetry in an alloy unit cell depends largely on the modulation frequency and the phase angle difference between the potential modulation and the flow fluctuation, when both modulations occur at the same frequency.

Dimensionless groups are developed to provide guidelines for designing an electrolyte that has the necessary properties for inducing large-amplitude composition variations in periodically-plated alloys. It is shown that operating the deposition process with one mass-transfer-limited species (i.e., the dimensionless group $K_{c,1}Sc^{-1/3} \gg 1$) and one activation-limited species (i.e., the dimensionless group $K_{c,2}Sc^{-1/3} \ll 1$) produces CMA's when the flow is modulated, the potential is modulated, or both flow and potential are modulated simultaneously. Anodic dissolution of the alloy is unimportant for the kinetic parameters studied here, because the dimensionless groups $K_{a,1}Sc^{-1/3}$ and $K_{a,2}Sc^{-1/3}$ are both negligibly small (i.e., $K_{a,1}Sc^{-1/3} \ll 1$ and $K_{a,2}Sc^{-1/3} \ll 1$).

There appears to be a lack of research investigating the material properties of nanometer-wavelength, asymmetric, composition-modulated alloys. This may be due to the difficulty of fabricating short-wavelength materials with well-controlled asymmetries. The results in this paper suggest that it is possible to form asymmetric, composition-modulated alloys with well-defined and well-controlled graded junctions eletrochemically. Such materials may possess unusual material properties.

Finally, one must keep in mind that we have not addressed the issue of alloy stability in this paper. The composition profiles presented in this paper do not account for solid-state redistribution. Interdiffusion, spinodal decomposition or ordering of the alloy may occur depending upon the thermodynamic properties of the solid-state alloy solution. Hilliard (1970) provides a thorough review of the kineitcs and thermodynamics of alloy interdiffusion.

## Acknowledgments

Support for this research was provided in part by grants from the San Diego Supercomputing Center, Eastman Kodak Corporation, and a University of California, Davis Graduate Research Award. DTS also thanks the Electrochemical Society for its support through the Colin Garfield Fink Fellowship.

## Appendix A

The nonsinusoidal composition profiles shown in Figures 2 and 5-9 are due in part to higher harmonic components in the species fluxes of each depositing species. The higher harmonic flux components arise from nonlinearity in the governing equations and the exponential potential dependence in the kinetic boundary conditions. Higher harmonic response can be quantified by decomposing the time periodic flux of $Cu^{+2}$ and $Ni^{+2}$ at the RDE surface into its Fourier components. Table A1 lists the magnitudes of the first 10 Fourier modes for the dimensionless species fluxes, defined by

$$\left[\frac{D_i c_{\infty i}}{D_{Cu} c_{\infty Cu}}\right] \frac{\partial C_i}{\partial \eta}(\tau, 0) = A^{(0)} + A^{(1)} \cos(p\tau - \varphi) + A^{(2)} \cos(2pt - \varphi) + \cdots \quad \text{(A1)}$$

where $i$ is either Cu or Ni. Three cases are considered in Table A1. Case i corresponds to the conditions given for curve 1 in Figure 2. The flow is modulated and the potential is held constant. Case ii corresponds to the conditions given for curve 1 in Figure 6. The potential is modulated and the flow is steady. Case iii corresponds to the conditions given for the $\phi = 90°$ curve in Figure 7. The flow and potential are both modulated simultaneously.

The results in Table A1 show the presence of higher harmonic response for each case presented. As noted earlier, varying the speed of the RDE introduces higher harmonic response through the governing equations and modulating the potential introduces higher harmonic response through the Butler-Volmer kinetic rate expression. Comparing the Fourier modes for cases i and ii in Table A1 provides quantitative insight into the relative importance of each source of higher harmonics.

In case i, the first harmonic is dominant and the response in the higher harmonics drops off rapidly with each progressive harmonic. In case ii, each successive harmonic does not decay rapidly. Clearly, higher harmonics introduced through the

**Table A1. Harmonics of Dimensionless Flux for Three Cases***

| $\left(\frac{c_{oi}}{c_{o\mathrm{Cu}}}\right)\frac{\partial C_i}{\partial \eta}(\tau, 0)$ | Mean | $A^{(1)}$ | $A^{(2)}$ | $A^{(3)}$ | $A^{(4)}$ | $A^{(5)}$ | $A^{(6)}$ | $A^{(7)}$ | $A^{(8)}$ | $A^{(9)}$ | $A^{(10)}$ |
|---|---|---|---|---|---|---|---|---|---|---|---|
| Case i | | | | | | | | | | | |
| $i$ = Cu | 5.636 | 2.964 | 0.413 | 0.144 | 0.076 | 0.044 | 0.026 | 0.015 | 0.008 | 0.005 | 0.002 |
| $i$ = Ni | 1.352 | 0.000 | 0.000 | 0.000 | 0.000 | 0.000 | 0.000 | 0.000 | 0.000 | 0.000 | 0.000 |
| Case ii | | | | | | | | | | | |
| $i$ = Cu | 6.012 | 0.007 | 0.005 | 0.003 | 0.001 | 0.001 | 0.000 | 0.000 | 0.000 | 0.000 | 0.000 |
| $i$ = Ni | 23.933 | 42.122 | 29.069 | 16.106 | 7.330 | 2.788 | 0.893 | 0.239 | 0.052 | 0.008 | 0.002 |
| Case iii | | | | | | | | | | | |
| $i$ = Cu | 5.631 | 2.963 | 0.412 | 0.147 | 0.074 | 0.044 | 0.025 | 0.014 | 0.008 | 0.005 | 0.003 |
| $i$ = Ni | 23.911 | 42.075 | 29.017 | 16.053 | 7.281 | 2.748 | 0.865 | 0.222 | 0.042 | 0.003 | 0.002 |

Case i, modulated flow and steady potential with conditions identical to curve 1 in Figure 2
Case ii, steady flow and modulated potential with conditions identical to curve 1 in Figure 6
Case iii, modulated flow and potential with conditions identical to curve $\phi = 90°$ in Figure 7

boundary conditions are larger than the harmonics that arise from the governing equations.

Comparing cases i and ii with case iii shows that the $Cu^{+2}$ flux and the $Ni^{+2}$ flux are independent of each other. Fluctuating flow does not significantly change the $Ni^{+2}$ flux in going from case ii to case iii, since $K_{c,\mathrm{Ni}}Sc^{-1/3} \ll 1$. Moreover, potential modulation does not affect the $Cu^{+2}$ flux in going from case i to case iii since $K_{c,\mathrm{Cu}}Sc^{-1/3} \gg 1$.

## Notation

$a$ = activity
$c$ = concentration, mol/m$^3$
$C$ = dimensionless concentration
$D$ = species diffusivity, m$^2$/s
$e$ = unit vector
$e^-$ = electron
$E$ = electrode potential vs. NHE, V
$F$ = Faraday's constant, 96,485 C/equiv.
$f$ = radial flow function or $F/RT$
$F$ = dimensionless radial flow function
$fwhm$ = alloy full width at half maximum
$g$ = azimuthal flow function, rad/s
$G$ = dimensionless azimuthal flow function
$h$ = axial velocity, m/s
$H$ = dimensionless axial velocity
$i$ = current density, A/m$^2$
$k_c$ = electrochemical cathodic rate constant
$k_a$ = electrochemical anodic rate constant, mol/m$^2$ · s
$K$ = dimensionless kinetic parameter
$L$ = alloy periodicity wavelength, nm
$M$ = metal
$m$ = molecular weight, kg/mol
$n$ = number of electrons transferred
$p$ = dimensionless frequency
$r$ = radial coordinate, m
$Sc$ = Schmidt number
SLOPE 1 = maximum alloy composition gradient
SLOPE 2 = minimum alloy composition gradient
$t$ = time, s
$U_{\mathrm{ref}}$ = potential difference between a reference electrode and a NHE, V
$V$ = electrode potential vs. SCE, V
$v$ = velocity vector, m/s
$Z$ = axial coordinate, m

### *Greek letters*

$\alpha$ = angular velocity modulation amplitude
$\beta$ = kinetic symmetry coefficient
$\Delta$ = difference or change
$\eta$ = dimensionless axial coordinate
$\nu$ = kinematic viscosity, m$^2$/s
$\Omega$ = angular velocity, rad/s
$\Lambda$ = dimensionless alloy periodicity wavelength
$\zeta$ = alloy unit cell distance
$\rho$ = alloy mass density, kg/m$^3$
$\rho_o$ = electrolyte mass density, kg/m$^3$
$\phi$ = modulation phase angle difference
$\sigma$ = modulation frequency, rad/s
$\tau$ = dimensionless modulation period

### *Subscripts*

$s$ = surface quantity
$r$ = radial direction
$o$ = refernce or mean value
$\theta$ = aximuthal direction
$z$ = axial direction
$\infty$ = bulk quantity
$i$ = species $i$
$c$ = cathode
$a$ = anode
Ni = nickel
Cu = copper

### *Superscripts*

$\bullet$ = fixed reference frame
$n_i^+$ = species $i$ charge
$o$ = reduced species

## Literature Cited


Bard, A. J., and L. R. Faulkner, *Electrochemical Methods*, Wiley, New York (1980).

Bennett, L. H., D. S. Lashmore, M. P. Dariel, M. J. Kaufman, M. Rubinstein, P. Lubitz, O. Zadok, and J. Yahalom, "Magnetic Properties of Electrodeposited Copper-Nickel Composition-Modulated Alloys," *J. Magn. Magn. Mat.*, **67**, 239 (1987).

Brownlow, J. M., "Electrodeposition of Thin Magnetic Films in the Ni-Fe-Cu System," *J. Appl. Phys.*, **38**, 1440 (1967).

Cohen, U., F. B. Koch, and R. Sard, "Electroplating of Cyclic Multilayered Alloy (CMA) Coatings," *J. Electrochem. Soc.*, **130**, 1987 (1983).

Cohen, U., K. R. Walton, and R. Sard, "Development of Silver-Palladium Alloy Plating For Electrical Contact Applications," *J. Electrochem. Soc.*, **131**, 2489 (1984).

Dariel, M., L. H. Bennett, D. S. Lashmore, P. Lubitz, M. Rubinstein, W. L. Lechter, and M. Z. Harford, "Properties of Electrodeposited Co-Cu Multilayer Structures," *J. Appl. Phys.*, **61**, 4067 (1987).

Deslouis, C., C. Gabrielli, and B. Tribollet, "An Analytical Solution of the Nonsteady Convective Diffusion Equation for Rotating Electrodes," *J. Electrochem. Soc.*, **130**, 2044 (1983).

Hilliard, J. E., "Spinodal Decomposition," *Phase Transformations*, H. I. Aaronson, ed., Amer. Soc. for Metals, 497 (1970).

Jankowski, A. F., and T. Tsakalakos, "Mechanical Properties of Cu-Ni-Fe Thin Films," *Layered Structures, Epitaxy, and Interfaces,* J. M. Gibson and L. R. Dawson, eds., **37,** Materials Research Society, 529 (1985).

Lashmore, D. S., and M. P. Dariel, "Electrodeposited Cu-Ni Textured Superlattices," *J. Electrochem. Soc.,* **135,** 1218 (1988).

Menezes, S., and D. Anderson, "Electrodeposition and Characterization of Multilayered Cu-Ni Ultrastructures," *Extended Abstracts,* Meeting of the Electrochem. Soc., **88-2,** 503 (1988).

Miller, B., and S. Bruckenstein, "Submicromolar Analysis with Rotating and Hydrodynamically Modulated Disk Electrodes," *Anal. Chem.,* **46,** 2026 (1974).

Nagia, Y., M. Senda, and T. Toshima, "Properties of Ion-Beam-Sputtered Ni/Fe Artificial Lattice Film," *J. Appl. Phys.,* **63,** 1136 (1988).

Newman, J., *Electrochemical Systems,* Prentice-Hall, Englewood Cliffs, NJ (1973).

Pesco, A. M., and H. Y. Cheh, "Current and Composition Distributions During the Deposition of Tin-Lead Alloys on a Rotating Disk Electrode," *J. Electrochem. Soc.,* **135,** 1722 (1988).

Puippe, J. Cl., and N. Ibl, "Influence of Charge and Discharge of Electric Double Layer in Pulse Plating," *J. Appl. Electrochem.,* **10,** 775 (1980).

Rosebrugh, T. R., and W. Lash Miller, "Mathematical Theory of the Changes of Concentration at the Electrode, Brought About by Chemical Reaction," *J. Phys. Chem.,* **14,** 816 (1910).

Ruffoni, A., and D. Landolt, "Pulse-Plating of Au-Cu-Cd Alloys: II. Theoretical Modelling of Alloy Composition," *Electrochim. Acta,* **33,** 1281 (1988).

Saraby-Reintjes, A., and M. Fleischmann, "Kinetics of Electrodeposition of Nickel From Watts Bath," *Electrochim. Acta,* **29,** 557 (1984).

Schwartz, D. T., P. Stroeve, and B. G. Higgins, "Fourier Transform Methods in Hydrodynamic Modulation Voltammetry," *J. Electrochem. Soc.,* **136,** in press (1989).

Schwartz, D. T., "Electrodeposition of Alloys in a Fluctuating Flow Field," PhD Thesis, Univ. of Claifornia, Davis (1989a).

Schwartz, D. T., "Multilayered Alloys Induced by Fluctuating Flow," *J. Electrochem. Soc.,* **136,** 53C (1989b).

Slonczewski, J. C., B. Petek, and B. E. Argyle, "Micromagnetics of Laminated Permalloy Films," *IEEE Trans. Magn.,* **MAG-24,** 2045 (1988).

Tench, D., and J. White, "Enhanced Tensile Strength for Electrodeposited Ni-Cu Multilayered Composite," *Metall. Trans. A,* **15A,** 2039 (1984).

Thaler, B. J., J. B. Ketterson, and J. E. Hilliard, "Enhanced Magnetization Density of a Composition Modulated Cu-Ni Thin Film," *Phys. Rev. Lett.,* **41,** 336 (1978).

Tribollet, B., and J. Newman, "The Modulated Flow at a Rotating Disk Electrode," *J. Electrochem. Soc.,* **130,** 2016 (1983).

Tsakalakos, T., and A. F. Jankowski, "Mechanical Properties of Composition Modulated Metallic Foils," *Ann. Rev. Mat. Sci.,* **16,** 293 (1986).

Verbrugge, M. W., and C. W. Tobias, "A Mathematical Model for the Periodic Electrodeposition of Multicomponent Alloys, " *J. Electrochem. Soc.,* **132,** 1298 (1985).

Verbrugge, M. W., and C. W. Tobias, "The Periodic, Electrochemical Codeposition of Cadmium and Tellurium," *AIChE J.,* **33,** 628 (1987).

White, R., and J. Newman, "Simultaneous Reactions on a Rotating-Disk Electrode," *J. Electroanal. Chem.,* **82,** 173 (1977).

Yahalom, J., and O. Zadok, "Formation of Composition-Modulated Alloys by Electrodeposition," *J. Mat. Sci.,* **22,** 499 (1987).

*Manuscript received Mar. 8, 1989, and revision received May 23, 1989.*